Published in final edited form as:
Nat Cell Biol. 2017 August ; 19(8): 928–940. doi:10.1038/ncb3574.

Endothelial Notch signalling limits angiogenesis via control of artery formation

Sana S. Hasan[1,2], **Roman Tsaryk**[1,2], **Martin Lange**[1,2], **Laura Wisniewski**[1,2], **John C. Moore**[3], **Nathan D. Lawson**[3], **Karolina Wojciechowska**[4], **Hans Schnittler**[2,5], and **Arndt F. Siekmann**[1,2,*]

[1]Max Planck Institute for Molecular Biomedicine, Röntgenstrasse 20, D-48149 Münster, Germany [2]Cells-in-Motion Cluster of Excellence (EXC 1003 – CiM), University of Muenster, Muenster, Germany [3]Department of Molecular, Cell, and Cancer Biology, University of Massachusetts Medical School, 364 Plantation Street, Worcester, MA 01605 [4]University of Warsaw, Faculty of Biology, Ul. Miecznikowa 1, 02-096 Warsaw, Poland [5]Institute of Anatomy and Vascular Biology, Westfälische Wilhelms-Universität Münster, Vesaliusweg 2-4, 48149 Münster, Germany

Abstract

Angiogenic sprouting needs to be tightly controlled. It has been suggested that the Notch ligand *dll4* expressed in leading tip cells restricts angiogenesis by activating Notch signalling in trailing stalk cells. Here, we show using live imaging in zebrafish that activation of Notch signalling is rather required in tip cells. Notch activation initially triggers expression of the chemokine receptor *cxcr4a*. This allows for proper tip cell migration and connection to the pre-existing arterial circulation, ultimately establishing functional arterial-venous blood flow patterns. Subsequently, Notch signalling reduces *cxcr4a* expression, thereby preventing excessive blood vessel growth. Finally, we find that Notch signalling is dispensable for limiting blood vessel growth during venous plexus formation that does not generate arteries. Together, these findings link the role of Notch signalling in limiting angiogenesis to its role during artery formation and provide a framework for our understanding of the mechanisms underlying blood vessel network expansion and maturation.

Keywords

zebrafish; angiogenesis; imaging; Notch signalling; artery; vein; blood flow; cxcr4

*Corresponding author: Dr. Arndt F. Siekmann, arndt.siekmann@mpi-muenster.mpg.de, phone: +49 251 70365 459.

Author Contributions

S.S.H. and A.F.S. designed the experiments, performed experiments, analysed the data and wrote the manuscript. M.L. performed in situ hybridization and analysed data. R.T. performed HUAEC experiments, qPCR analysis and ChIP. L.W. analysed data. K.W. analysed data. J.C.M. and N.D.L. provided the fli1b antibody. H.S. provided HUAEC.

Competing Financial Interests

The authors declare no competing financial interests.

Data availability. All data supporting the findings of this study are available from the corresponding author on reasonable request.

Europe PMC Funders Author Manuscripts

The formation of a functional vasculature entails the initial sprouting of new blood vessels and the subsequent development of properly connected arteries and veins. Despite the importance of these processes, we still lack an understanding of the mechanisms balancing blood vessel expansion with artery-vein maturation and the establishment of efficient blood flow patterns. Previous studies have shown that Notch signalling controls angiogenic growth by determining the positions of endothelial cells in growing blood vessel sprouts1–3. In this setting, vascular endothelial growth factor (VEGF) triggers expression of the Notch ligand *dll4* in leading tip cells4–6, which in turn activates Notch signalling in trailing stalk cells, thereby preventing the formation of supernumerary tip cells7–10. Studies using embryoid bodies suggested that endothelial cells (EC) compete for the tip cell position during blood vessel sprouting4. Furthermore, Notch signalling is essential for arterial differentiation in zebrafish11, 12 and mouse embryos13–15 prior to the onset of blood flow. Intriguingly, several tip cell enriched genes, such as *Dll4*7, *Cxcr4*16, 17 or *Apelin*18, 19 display an arterial restricted expression pattern, raising the possibility that tip cell and arterial fate specification might be coupled. Time lapse imaging of blood vessel sprouting in zebrafish and genetic lineage tracing in mice showing that vein-derived tip cells contribute to newly forming arteries20 further supported this notion. However, to date it is not clear if Notch signalling can simultaneously control tip cell specification and artery formation. In addition, we only have an incomplete understanding of the Notch downstream signalling molecules in ECs that might mediate these processes.

One key molecule influencing EC migration during angiogenesis is the chemokine receptor *cxcr4a*21, 22, 23, 24. In the early zebrafish embryo16, 25, 26 and during tissue regeneration20, *cxcr4a* is important for arterial morphogenesis. It also has a role in guiding the formation of the coronary arteries27, 28 and controls artery-nerve alignment in the mouse skin29. Despite the importance of CXCR4 function in these different vascular beds, it is still not clear which signalling pathways control *CXCR4* expression in sprouting ECs.

Here we show, using time-lapse imaging in zebrafish embryos, that endothelial tip cells activate the Notch signalling pathway during blood vessel sprouting. We identify the chemokine receptor *cxcr4a* as an important Notch target during this process. Initially, Notch signalling induces *cxcr4a* expression, allowing proper tip cell migration towards the arterial circulation, thereby establishing optimal blood flow. At later stages, we observe downregulation of *cxcr4a* expression via Notch signalling and blood flow, which is important to prevent blood vessel hypersprouting. Together, our results not only link the role of Notch signalling during artery formation to its role in restricting angiogenesis, but also elucidate a complex regulatory interplay between Notch and *cxcr4a* signalling.

Results

Live imaging reveals activation of Notch signalling in endothelial tip cells

In order to investigate Notch signalling during angiogenic sprouting in real time, we chose to study the development of the ocular vasculature in zebrafish embryos (Fig. 1a). In this setting, ECs sprout from the venous primordial midbrain channel (PMBC) and connect to the cranial division of the carotid artery (CrDI), ultimately forming the nasal ciliary artery (NCA)30–32. The main Notch ligand in the vasculature is *dll4*1. We developed a *dll4*

reporter transgenic line *Tg(dll4:gal4)*^{mu106}; *Tg(UAS:GFP)*^{nkuasgfp1a}. We detected a good correlation between *dll4* mRNA, GFP mRNA and protein in ECs (Supplementary Fig. 1a, b). We then combined this line with *Tg(kdrl:NLS-mcherry)*^{is4}, which labels all EC nuclei, and performed time-lapse imaging for 12 hours (h; Supplementary Videos 1-3, see also Supplementary Fig. 1c-f). *dll4* expression initiated in the leading tip cell (Fig. 1a, cell 1, 2:36 h time point, c) followed by activation of the reporter line in stalk cells (cells 2 and 3, starting at the 5:12 h time point). By contrast, we did not find *dll4* expression in cells which kept the connection to the PMBC (Fig. 1a, cell 4, 9:58 h time point, c). Expression of *dll4* was also detected in the CrDI, the blood vessel to which the NCA connected (Fig. 1a, arrows) and was still detected in both vessels 12 h after their fusion (50 hpf time point, Supplementary Fig. 2a). NCA sprouting and *dll4* expression required VEGF signalling (Supplementary Fig. 2c-f). Therefore, in agreement with previous results in the mouse retina5, 7, 10, 33, 34, our analysis revealed that *dll4* became activated in tip cells of growing blood vessel sprouts in the zebrafish eye.

We next analysed activation of Notch signalling during the same time frame, using an established Notch indicator line, *Tg(TP1:GFP)*^{um14} 35 (Fig 1b, d, Supplementary Videos 4-6, Supplementary Fig. 2g-j). We expected to observe Notch activation in trailing stalk cells. Surprisingly, Notch activation was first initiated in the leading tip cell (Fig. 1b, 6:15 h time point, d) and increased over time (Fig. 1b, 9:10 h time point, d). Subsequently, trailing cells were also marked by EGFP in the Notch indicator line (Figure 1b, 9:10 h time point, cells 2 and 3, d). We observed Notch pathway activation several hours after the onset of *dll4* expression (compare Fig. 1c, 1d). We further noted that ECs within the NCA showing Notch pathway activation fused to the Notch positive CrDI (Fig. 1b, arrows). Both vessels remained Notch positive at 12 h after fusion (50 hpf time point, Supplementary Fig. 2b). To detect possible fluctuations in Notch pathway activation, we analysed *Tg(TP1bglob:VenusPEST)*^{s940} embryos36, in which the PEST domain reduces fluorescent protein half life37. These embryos also displayed stable activation of the Notch pathway within tip cells (Supplementary Fig. 3, Supplementary Videos 7-9). Finally, we generated *Tg(dll4:gal4)*^{mu106}; *Tg(UAS:GFP)*^{nkuasgfp1a}; *Tg(TP1:H2B-mcherry)*^{s939} triple transgenic embryos to image *dll4* expression and Notch pathway activation simultaneously. These embryos comparably showed activation of *dll4* expression followed by Notch pathway activation in leading NCA tip cells (Supplementary Fig. 4, Supplementary Videos 10-12). Thus, our results show that expression of *dll4* precedes Notch activation and that Notch signalling initially occurs in tip cells prior to pathway activation in stalk cells (Fig. 1e).

Notch signalling occurs in trans

Knockdown of *dll4* led to an almost complete absence of *Tg(TP1:GFP)*^{um14} activation (Fig. 2a, b, Supplementary Fig. 5a-d, Supplementary Videos 13-15), showing that Dll4 is the relevant endothelial Notch ligand. Notch signalling can occur in trans or in cis38, 39. In order to distinguish between these possibilities, we transplanted *dll4* knockdown cells that were also transgenic for the Notch indicator line into wildtype (wt) embryos (Fig. 2c). In the case of cis-activation, we would expect to observe absence of Notch activation within *dll4*-deficient tip cells, while activation in trans would allow for Notch activation from neighbouring, *dll4* positive host endothelial cells (Fig. 2d). We observed Notch pathway

activation in *dll4* knockdown tip cells when they were in association with wt host cells (Fig. 2e-k; Supplementary Fig. 5e-v). Thus, our results suggest that Notch pathway activation in tip cells occurs in trans.

Notch ligand deficient cells can maintain tip cell positions

These transplantation experiments furthermore revealed an unexpected ability of ECs lacking *dll4* to occupy tip cell positions. Previous studies proposed that ECs shuffle between tip and stalk positions during angiogenic sprouting and that these behaviours depend on Notch activity in trailing stalk cells4. According to this model, *dll4*-deficient cells would be excluded from the tip position (Fig. 3a). To corroborate our findings in mosaic NCAs, we examined the distribution of either control or *dll4* morpholino injected *Tg(kdrl:EGFP)*^{s843} donor cells within sprouting intersegmental blood vessels (ISVs) (Fig. 3b). This analysis revealed that control (Figure 3c, arrowhead, d) and *dll4* morpholino (Fig. 3c, arrow, d) injected donor cells were equally distributed between tip and stalk cell positions. In order to investigate whether cell shuffling took place during ISV sprouting, we performed time-lapse analysis of mosaic embryos. These videos showed that *dll4* deficient cells could remain in tip cell positions throughout the sprouting process (Fig. 3e, arrowheads, see also Supplementary Fig. 6a-d). Of note, and in agreement with a recent publication40, we also did not detect EC shuffling during ISV sprouting in wt embryos (Supplementary Fig. 6h, i).

Several Notch ligands are expressed in zebrafish ECs, which could potentially activate Notch receptors in the absence of *dll4* function. We therefore analysed the distribution of *mindbomb* (*mib*) mutant donor cells. *Mib* mutants lack an essential ubiquitin ligase necessary for Notch ligand processing41. We observed that *mib* mutant cells were also equally distributed between tip and stalk cell positions during ISV sprouting (Fig. 3f, g, Supplementary Fig. 6e-g). Together, these results indicate that Notch ligand deficient cells can occupy tip cell positions during blood vessel sprouting at a similar frequency as wt cells.

Loss of Notch signalling impairs the connection of new blood vessel sprouts to the existing arterial vasculature

Based on our observations that Notch signalling is activated within tip cells, we hypothesized that interfering with Notch signalling might compromise tip cell biology. Previous studies showed that Notch signalling controls EC proliferation and vascular expansion5, 7–10, 42. In agreement, we found that NCA area and cell numbers were increased in embryos lacking *dll4* function (Fig. 4a-c). However, we also detected that NCA-forming cells displayed aberrant migratory behaviours and improper connection to the CrDI (Fig. 4a, arrowheads, 4d, Supplementary Videos 13-15). This ultimately led to a direct connection between two veins and aberrant NCA blood flow patterns that lacked proper arterial input (Fig. 4e-h). Therefore, Notch activation regulates EC migration (Fig. 4i, j).

Notch regulation of *cxcr4a* expression is responsible for establishing arterial connections

We speculated that Notch signaling might regulate the expression of the chemokine receptor *cxcr4a* due to the reported roles of CXCR4 in cell migration and arterial morphogenesis21, 22. We detected *cxcr4a* expression in sprouting NCA cells (Fig. 5a, 28 and 32 hpf time points, arrows). In agreement with the regulation of *cxcr4a* expression by hemodynamic

forces16, 43, we observed downregulation of *cxcr4a* expression at the 38 hours post fertilization (hpf) time point (Fig. 5a), when the NCA displayed blood flow. The expression of *cxcr4a* was almost completely absent in newly sprouting ECs in *dll4* morpholino injected embryos between 28 and 38 hpf (Fig. 5b, arrows). This indicates that Notch signalling can positively regulate *cxcr4a* expression.

We reasoned that if lack of *cxcr4a* expression was responsible for the observed failure of NCA cells to connect to the CrDI in embryos lacking proper Notch signalling, then *cxcr4a* mutants should recapitulate this phenotype. Analysis of *cxcr4a* mutant zebrafish showed an absence of NCA-CrDI connection at the 36 hpf time point (Fig. 5c, arrows). By 48 hpf, the NCA in wt embryos carried blood flow (Fig. 5c, 48 hpf time point, bracket, Supplementary Fig. 7a, b, Supplementary Videos 16-17), while *cxcr4a* mutants displayed a dysmorphic NCA still lacking CrDI connection (Fig. 5c, 48 hpf time point, bracket, 5d, Supplementary Videos 18 and 19). Analysis of EC numbers in *cxcr4a* mutants revealed no significant difference between siblings and mutants (Fig. 5e, f). Therefore, loss of *cxcr4a* function recapitulated the migratory phenotype of NCA cells in embryos lacking *dll4*-Notch signalling without affecting EC (Fig. 5g, h; Supplementary Fig. 7c, d). Together, our findings suggest that Notch signalling induces *cxcr4a* expression during angiogenic sprouting.

Loss of *cxcr4a* function rescues hypersprouting phenotype in Notch deficient blood vessels

We next wanted to examine whether the observed regulation of *cxcr4a* expression via Notch signalling was a general phenomenon. We therefore analysed *cxcr4a* expression in newly forming intersegmental blood vessel sprouts (ISVs). We detected *cxcr4a* expression in the dorsal aorta and in sprouting ISVs (Fig. 6a, 28 and 32 hpf time points, arrows). However, at later stages and after the onset of blood flow (2.5 dpf time point)44, we observed downregulation of *cxcr4a* expression in ISVs and in the DLAV (Fig. 6a, 2.5 dpf time point, arrow). By contrast, *dll4* morpholino injected embryos showed an initial reduction of *cxcr4a* expression (Fig. 6b, arrows, 28 and 32 hpf time-points), as we had observed in the eye vasculature. However, at later stages, *cxcr4a* expression was upregulated (Fig. 6b, 2.5 dpf time-point, arrows).

Motivated by these observations, we explored possible genetic interactions between Notch and *cxcr4a* signalling. In order to do so, we knocked down *dll4* in homozygous *cxcr4a* mutants. Of interest, while the amount of ectopic sprouts (Fig. 6c, arrows, e) was strongly reduced in *dll4* knockdown embryos lacking *cxcr4a* function, EC numbers were still increased (Fig. 6f). *cxcr4a*/*dll4* double mutant embryos showed a similar rescue of hypersprouting (Fig. 6d, g, h). Thus, our results show that the hyperangiogenesis phenotype observed in *dll4* knockdown embryos is partly due to an increase of *cxcr4a* expression.

To investigate the mechanism by which loss of Notch signalling might influence *cxcr4a* expression, we examined ISV blood flow patterns in *dll4* knockdown embryos. As previously reported8, we observed a reduction of ISVs carrying blood flow, both at the 54 hpf and at the 72 hpf time points (Supplementary Fig. 7e-h). More than 90% of ISVs showing ectopic blood vessel sprouts at 72 hpf did not carry circulation at the 54 hpf time

point, while of the ISVs showing no ectopic sprouts, only 60% did not carry blood flow at the 54hpf time point (Supplementary Fig. 7g). At the 72 hpf time point, almost 80% of ISVs with ectopic sprouts still did not carry blood flow, while only 60% of ISVs without ectopic sprouts did not carry blood flow. We also detected a marked increase in *cxcr4a* mRNA in the DA and in the DLAV when we blocked blood flow between 48 and 52 hpf (Supplementary Fig. 7h). Together, our findings indicate that Notch signalling differentially regulates *cxcr4a* expression and that there is a genetic interaction, which may be direct or indirect, between both pathways. They furthermore suggest that aberrant blood flow patterns contribute to increases in *cxcr4a* expression in *dll4* deficient embryos.

Notch signalling differentially regulates *cxcr4* expression

Using a Human Umbilical Artery Endothelial Cell (HUAEC) culture system, in which Notch signalling was activated by plating cells on DLL4, we found *CXCR4* upregulation between 4 and 8 h of incubation (Fig. 7a). This was unexpected, as previous studies showed that Notch signalling negatively regulates *CXCR4* expression in ECs45, 46. However, when we exposed HUAEC to DLL4 for longer times (24 h), we observed a comparable downregulation of *CXCR4* expression (Fig. 7a). Thus, Notch signalling can differentially regulate *CXCR4* expression in cultured ECs, depending on the duration of Notch pathway activation.

In order to further explore this aspect of Notch signalling, we analysed *CXCR4* regulatory regions. This analysis identified 3 RBPJ bindings sites, the downstream transcription factor of the Notch signalling pathway38, (Fig. 7b), of which site 2 is being conserved among mammals (see materials and methods). We then performed Chromatin Immunoprecipitation (ChIP) in basal conditions and 4 h after DLL4 mediated Notch pathway activation. As a control, we used a previously described RBPJ binding site in the *HES4* promoter (Fig. 7c). Surprisingly, all RBPJ binding sites within *CXCR4* regulatory regions showed strong enrichment already in basal conditions (Fig. 7d). Subsequent to Notch pathway activation, there was a trend towards reduction in enrichment, although this was not statistically significant (Fig. 7d). Control regions 5’ and 3’ of the *CXCR4* promoter did not show enrichment (Fig. 7d). Thus, our analysis uncovers 3 RBPJ binding sites that might control *CXCR4* expression. It furthermore suggests that these sites are differentially occupied by RBPJ depending on Notch signalling status.

To determine the significance of each site for *CXCR4* expression, we generated a luciferase construct containing 2.5 KB upstream of the *CXCR4* start codon, as well as the first intron. In keeping with our qPCR results, Notch pathway activation led to an increase in luciferase expression (Fig. 7e). Mutating RBPJ binding site 1 caused a small reduction of luciferase expression, while mutating the conserved RBPJ binding site 2 increased luciferase expression already in basal conditions. These results suggest that RBPJ acts as a transcriptional repressor and that Notch pathway activation might release this repressive activity. However, we noted that Notch pathway activation still increased luciferase expression irrespective of functional RBPJ binding sites. This might argue for the existence of other indirect mechanisms downstream of Notch signalling controlling *CXCR4* expression.

To investigate whether Notch signalling can directly influence *cxcr4a* expression during angiogenesis, we generated triple transgenic embryos *Tg(cdh5:gal4ff)*^{mu101}*; (UAS:GFP)*^{nkuasgfp1a}*; (UAS:myc-NICD)*^{kca3}. In these embryos, myc-tagged Notch intracellular domain (NICD) is specifically expressed in the vasculature, albeit in a mosaic fashion. We also injected these embryos with *dll4* MO. 85 % of myc+ ECs in ISV sprouts showed *cxcr4a* expression (Fig. 7f, arrows, g) compared to only 15% of myc- ECs (Fig 7f, asterisk, g), thus suggesting a cell autonomous role of Notch signalling in inducing *cxcr4a* expression. Together, our findings argue for an initially repressive function of RBPJ on the *CXCR4* promoter that might be relieved in a cell autonomous manner upon Notch pathway activation.

Notch signalling does not control venous blood vessel sprouting

Our results suggest that Notch signalling restricts angiogenesis in settings of coordinated artery formation. We therefore wanted to analyse whether Notch signalling also had a role during the expansion of a venous vascular plexus (Fig. 8a-c). Analysis of caudal vein plexus (CVP) formation in *dll4* morpholino injected embryos in comparison to control morpholino injected embryos (Fig. 8b and Supplementary Video 20) revealed normal migratory behaviours of ECs (Fig. 8c, 3:10 h time point, arrowheads, Supplementary Video 21), sprout fusion events (Fig. 8c, 5:17 h time point, arrowhead) and lumen formation (Fig. 8c, 7:08 h time point, arrowhead). In addition, we did not observe an increase in EC numbers or CVP area in *dll4* mutant embryos (Fig. 8d-f). Analysis of *Tg(TP1:GFP)*^{um14} embryos did not reveal activation of the Notch signalling pathway in these cells during CVP expansion (Fig. 8g). Correspondingly, we did not detect *dll4* reporter activity or *cxcr4a* mRNA expression in sprouting CVP cells (Supplementary Fig. 8a, b). These findings reveal that during CVP expansion, Notch signalling is not necessary to restrict angiogenic sprouting.

Discussion

In this report we used time-lapse imaging to examine the spatio-temporal sequence of Notch pathway activation within angiogenic blood vessel sprouts. Previous reports investigated activation of Notch signalling at fixed time points7, 31, 35. We now found that *dll4* expression preceded Notch pathway activation both in leading tip and subsequently in trailing stalk cells. These cells ultimately connected to a Notch-positive arterial blood vessel, thereby terminating the angiogenesis program. Our results therefore show how Notch pathway activation and artery formation are integrated during angiogenesis (Supplementary Fig. 8c, d). They help to explain how growing tissues can generate the appropriate amount of arteries, as these are continuously being generated from venous-derived tip cells that activate Notch signalling. These will subsequently be exposed to arterial blood flow patterns, which can induce the expression of arterial genes47.

These discoveries redefine the role of Notch signalling during angiogenesis in comparison to current models of blood vessel sprouting, where DLL4 from tip cells would activate Notch signalling in trailing stalk cells and prevent the formation of excessive tip cells (Supplementary Fig. 8c, d)2. Our work suggests important differences concerning Notch signalling pathway activation during blood vessel sprouting in distinct settings. We

previously suggested that tip cells in ISV sprouts lack Notch signaling9. However, this might be a special scenario, since ISVs do not sprout from a vein, but rather from an artery.

An outstanding unresolved question is why we do not observe activation of Notch signalling in stalk cells first, as tip cells express Dll4 prior to stalk cells. One potential explanation is that stalk cells are less competent to receive Notch signalling compared to tip cells, a possibility we are currently investigating. Alternatively, cis-inhibition38, where interaction between the ligand and the receptor present on the same cell leads to endocytosis and further degradation of the receptor–ligand complex might influence Notch pathway activation in tip and stalk cells.

Loss of Notch signalling leads to overproliferation of ECs and the formation of a hyperbranched vasculature. Previous studies showed that PTEN mediates the Notch induced proliferation arrest in ECs48. We now identify the chemokine receptor *cxcr4a* as another critical downstream target of Notch signalling, which specifically regulates cell migration. Thus, our work suggests that distinct target genes are responsible for the different phenotypes observed in angiogenic blood vessels lacking proper Notch signalling. We furthermore uncover temporal differences in *cxcr4* regulation by Notch. After an initial increase in expression, Notch signalling subsequently negatively regulates *cxcr4* expression. Our work reveals that the duality of this regulation is important, since early loss of *cxcr4a* causes migratory defects in tip cells, while ectopic expression at later stages contributes to excessive blood vessel sprouting. A better understanding of the regulatory modules that mediate the observed temporal differences in *cxcr4* expression downstream of Notch signalling will therefore be of great future interest.

A report analysing artery formation during angiogenic blood vessel sprouting in the mouse retina similarly found a role for Notch signalling in limiting *CXCR4* expression49. In addition, the authors provide evidence that also in this setting, Notch pathway activation in endothelial tip cells is necessary for these cells to incorporate into nascent arteries. Thus, the function of Notch signalling in regulating angiogenesis via artery formation appears to be conserved between mice and zebrafish. However, Pitulescu et al. did not observe an initial induction of *CXCR4* expression via Notch signalling. They propose that Notch signalling is rather required to limit endothelial VEGF mRNA levels, thereby secondarily affecting *CXCR4* expression. Future work will be necessary to better understand to which extend these observations reflect temporal or species specific differences in the control of *CXCR4* expression downstream of Notch pathway activation.

Ectopic *CXCR4* expression can be detected on tumour ECs46, which strongly respond to inhibition of Notch signalling50. Our findings will therefore also be of importance for improving treatments aiming at controlling blood vessel formation in pathological settings, when achieving correctly patterned vascular networks is a therapeutic aim.

Materials and Methods

Zebrafish strains

Zebrafish were maintained as described previously51. Embryos were staged by hours post fertilization (hpf) at 28.5°C52. The following transgenic lines were used: *Tg(kdrl:NLS-mcherry)*^{is4} 53, *Tg (dll4:gal4)*^{mu106} (this study), *Tg(UAS:GFP)*^{nkuasgfp1a} 54, *Tg(TP1:GFP)*^{um14} 55, *Tg(kdrl:H2B-EGFP)*^{mu122} 32, *Tg(kdrl:EGFP)*^{s843} 56, *Tg(fli:nEGFP)*^{y7} 57, *Tg(kdrl:Hsa.HRAS-mCherry)*^{s916} 58, *Tg(fli1a:EGFP)*^{y1} 59, *Tg(-0.8flt1:RFP)*^{hu5333} 60, *Tg(gata1:DsRed)*^{sd2} 61, *cxcr4a*^{um20} 26, *dll4*^{j16e1} 8, *mib*^{ta52b} 62, *Tg(TP1:Venus-PEST)*^{s940} 36, *Tg(TP1:H2B-mcherry)*^{s939} 36, *Tg(cdh5*^{BAC}*:gal4ff)*^{mu101} 16 abbreviated as *Tg(cdh5:GAL4)*^{mu101}, *Tg(UAS:myc-Notch1a-intra)*^{kca3} 63 abbreviated as *Tg(UAS:NICD)*^{kca3}.

Zebrafish used in this study were between 1 and 2 years of age and were not selected for gender. All animal experiments were performed in compliance with the relevant laws and institutional guidelines and were approved by local animal ethics committees of the Landesamt für Natur, Umwelt und Verbraucherschutz Nordrhein-Westfalen.

Generation of *Tg(dll4:gal4)*^{mu106} line

We applied BAC recombineering as described previously64, 65 using BAC CH211-19M2 and modified with a PCR-fragment amplified from pCS2+_Gal4FF_kanR using primers dll4_gal4FF_fw ctttctgggaatataatcgtgggtgacacggctgcccaggagaatcgaaaACCATGAAGCTACTGTCTTCTATCGAAC and dll4_kanR_rev: tgcgtcaaaacggtcgtgaaaaatgcgatgagaaaggtgagccaagctgcTCAGAAGAACTCGTCAAGAAGGCG

Live imaging, Confocal microscopy and Image processing

For in vivo imaging live embryos were mounted in 1% low melting point agarose in E3 embryo medium with 168 mg/l Tricaine (1X) for anaesthetization and 0.003% phenylthiourea to inhibit pigmentation. Imaging was carried out at SP5 or SP8 (Inverted) confocal microscopes using a 20x dry objective (Leica Microsystems). A heated microscope chamber at 28.5°C was used for recording time lapse videos. Stacks were taken every 15-25 min with a step size of 2.0 μm. Confocal stacks and time lapse videos were analysed using IMARIS Software (Bitplane) and ImageJ (NIH). Vessels in close proximity to the CrDI and NCA were cropped for better visualization.

Quantifications

To quantify the fluorescence intensity of the reporter lines for eye vessel live imaging experiments, surface rendering was performed around the endothelial cell nuclei using IMARIS software. The intensity of both red and green channels emitted from rendered nuclear surfaces was recorded over time. The green channel intensity value was divided by the red channel intensity value to normalize the data. Prism 6.0b (Graphpad) was used to plot graphs and for statistical analysis.

Morpholino injections

Morpholinos were obtained from Gene-Tools and dissolved in distilled water. Embryos were injected at one cell stage with 15 ng *dll4* morpholino (5'-CGAATCTTACCTACAGGTAGATCCG-3')9 or 5 ng of *kdrl* morpholino (5'-CCGAATGATACTCCGTATGTCAC-3')66. As a control, standard control morpholino (5'-CCTCTTACCTCAGTTACAATTTATA-3') was injected.

Fluorescence in situ hybridizations (FISH) with antibody staining

Whole mount FISH combined with EGFP antibody staining was performed in *Tg(kdrl:EGFP)*^{s843} line as described previously67. Double FISH was performed in the *Tg (dll4:gal4)*^{mu106};*(UAS:GFP)*^{nkuasgfp1a} embryos as described earlier68. The double FISH was followed by GFP antibody detection as described for the single FISH protocol. Previously described probes for *cxcr4a*26 and *dll4*9 were used. Images were acquired using SP5 or SP8 (Leica Microsystems) or LSM 780 (Zeiss) inverted confocal microscopes using a 20x dry objective.

Blastomere transplantation

Cell transplantation was performed as described9. About 30-40 cells were transplanted from donor embryos to the margin of host embryos at sphere stage. The endothelial cell contribution of transplanted cells was assessed by visualization of EGFP and m-cherry expression. Fli1b antibody staining was performed as described previously69.

Flow block experiments and inhibitor treatment

Flow block experiments were carried out as previously described16. The time of treatment was increased to 4 hours. VEGF inhibitor treatment was performed as described previously70. Corresponding amounts of DMSO were used to treat the control embryos.

Notch gain of function experiments

For Notch gain of function experiments *Tg(cdh5:GAL4)*^{mu101};*Tg(UAS:GFP)*^{nkuasgf1a} fish were crossed with *Tg(UAS:myc-NICD)*^{kca3} fish. Whole mount FISH combined with antibody staining for EGFP was performed as mentioned above. To detect NICD positive embryos, additional antibody was used against c-myc (1:250 dilution; Sigma-Aldrich M5546) followed by Alexa Fluor 647 (1:500 dilution; Invitrogen A-21236) goat anti-mouse secondary antibody staining during the FISH protocol.

Cell culture experiments

Human Umbilical Artery Endothelial cells (HUAEC) were isolated from umbilical cords of anonymized donors as described71 and according to the principles outlined in the Declaration of Helsinki; this was approved by the ethics board of the WW-University of Münster (2009–537-f-S). HUAEC were cultured in M200 medium with LSGS supplements (Invitrogen) and used for experiments until passage 5. For stimulation with DLL4, cell culture dishes (ibidi) were coated overnight at 4°C with 10 ug/ml DLL4 (R&D) diluted in PBS with 0.2% gelatin (Sigma). The cells were starved overnight in M200 medium supplemented with 0.1% FCS (Sigma) and reseeded on the dishes coated with DLL4 or only

gelatin in the starvation medium. . No cell lines used in this study were found in the database of commonly misidentified cell lines that is maintained by ICLAC and NCBI Biosample. The cell lines were not authenticated. The cell lines were not tested for mycoplasma contamination.

Quantitative Polymerase Chain Reaction (qPCR)

RNA was isolated with RNeasy Plus Micro kit (Qiagen) from HUAEC and reverse transcribed with iScript cDNA Synthesis Kit (BioRad). For qPCR, cDNA produced from 5 ng RNA and 8 pmol of each forward and reverse primer per reaction and Power SYBR Green PCR Master Mix (Applied Biosystems) were used. Relative expression was quantified by ΔΔCt method using RPL13A as an endogenous control. At each time point, the expression in control sample (cells grown on gelatin only) was set as 1 (0 on log2 scale). ΔCt values were used for statistical analysis. The following primers were used:

CXCR4-fwd: 5'-GCCCTCCTGCTGACTATTCC-3';

CXCR4-rev: 5'-GGCAGGATAAGGCCAACCAT-3';

RPL13A-fwd: 5'-TCGTACGCTGTGAAGGCATC-3';

RPL13A-rev: 5'-CAGCATACCTCGCACGGTC-3'.

Chromatin Immunoprecipitation (ChIP)

HUAEC were starved overnight in 0.1% FCS-containing medium and seeded on DLL4-coated or uncoated dishes in the same medium. After 4 h the cells were fixed with 1% formaldehyde for 5 min at room temperature. The cross-linking was stopped with 0.125 M glycine and after washing with cold PBS, cells were collected by scraping in PBS containing protease inhibitors. The cells were then resuspended in the nuclei lysis buffer (50 mM Tris-HCl pH 8.0, 10 mM EDTA, 1% SDS) and sonicated with Covaris S1 to obtain DNA fragments of 250 bp on average. Chromatin was diluted in and an aliquot was used to confirm sonication efficiency on Bioanalyzer (Agilent) and to quantify chromatin amount. 5 ug of chromatin were incubated with 2 ug RBPJ antibody (ab25949) overnight and then 50 ul of pre-washed Dynabeads-Protein G (Life Technologies) was added for 4 h to each reaction to pull down DNA/protein complexes. The beads were then washed 5 times with the buffers with increasing ionic strength and resuspended in the buffer containing 10 mM Tris-HCl pH8.0, 0.3 M NaCl, 5 mM EDTA pH8.0, 0.5% SDS. The beads were then incubated with RNase A at 65°C for 6 h and with Proteinase K at 55°C overnight. DNA was then isolated by phenol/chlorophorm extraction and ethanol precipitation and resuspenden in TE buffer. An aliquot of chromatin was saved as input and DNA was isolated in the same way. Input and ChIP DNA was used for qPCR using SYBR Green as described above. *HES4* primers (7273, Cell Signaling) were used as positive and alpha Satellite repeat primers (ab85782) as negative control. To identify potential RBPJ binding sites we analyzed *CXCR4* regulatory sequences with FIMO algorithm of the MEME Suite using SUH_HUMAN.H10MO.C matrix from HOCOMOCO database. In addition we investigated conservation of RBPJ binding sites between human and mouse using Mulan and multiTF

algorithms and V$RBPJK_01 matrix. The primers amplifying the regions containing RBPJ binding sites predicted by FIMO were:

CXCR4-1-fwd: 5'- GTAGAATCCTACAACTCTCCTCCCCATCT-3';

CXCR4-1-rev: 5'- ACCCTCAGCGTCTCAGTGCCCTT-3';

CXCR4-2-fwd: 5'- GCGTTGCAAAGACTCATTCTCCTAAA-3';

CXCR4-2-rev: 5'- CCAATATACCCCAAGCACCGAAG-3';

CXCR4-3-fwd: 5'- TGGTGGCTGGAAGAGGTTTCG-3';

CXCR4-3-rev: 5'- AAGAGATACGTAATGCAAGGCCTGT-3'.

In addition the primers to amplify the regions upstream and downstream of CXCR4 containing no predicted RBPJ binding sites were used:

CXCR4-4-fwd: 5'- CTGCACTCCAGCCTAACTGTCAGAG-3';

CXCR4-4-rev: 5'- TCCTATTCCTGGGAGCACACAAAA-3';

CXCR4-5-fwd: 5'- GGTTTAGATTAGGCTTCTCCAGACTGAA-3';

CXCR4-5-rev: 5'- ACAGCCCAGATGGGCGAAAG-3'.

The data were calculated as percent input and then normalized to negative region (alpha Satellite repeat) to obtain fold enrichment.

Luciferase Assay

For luciferase assays, we cloned a 2.5 kilo base upstream piece of the human *CXCR4* promoter including the first intron via PCR and restriction digest into pGL4.10 (Promega). The promoter piece was amplified with PfuII polymerase from a BAC containing the human *CXCR4* locus (IMGSB737B122186D; Source Bioscience) using primers Hs cxcr4 Pr 2.5 F (GGATGAACCAAAATCTTGTCAACTATTCCACTAACAGT) and Intron R (GTGGTCTGAGTCCCGAGGCAGCG) and subsequently cloned into pSC Blunt (Stratagene). The intron piece was amplified with primers Intron F (TGACGCCGAGGGCCTGAGTGCT) and Hs cxcr4 Bsp R (TTAATCATGATTTCCCCTGAGCCCATTTCCTCGGTGTAG) and cloned into pSC Blunt. The promoter piece was then digested using SpeI and Acc65I, while the intron piece was digested using Acc65I and BspHI and pGL 4.10 using NheI and NcoI. The three pieces were subsequently ligated together and confirmed via sequencing.

The predicted intronic RBPJ binding sites were mutated as follows: 5' site gcgtgggaaaa into gcgtCCgaC, the 3' site ctatgggaaaa into ctaCCggCTAa. We also mutated both sites simultaneously. Mutated nucleotides are shown in capital letters. The constructs were chosen to contain unique restriction sites (PflMI on the 5' end and AseI on the 3' end), leading to 776 BP fragments, which we custom ordered from MWG Biotech. The parental plasmid and the respective mutated construct were digested with PflMI and AseI and ligated.

HUAEC were starved in the medium with no FCS for 4 h and transfected for 45 min with *CXCR4* constructs using Lipofectamin 2000 and Plus Reagent (Invitrogen). Immediately after transfection the cells were reseeded in 0.1% FCS-containing medium on the dishes, pre-coated with DLL4 as described above. 24 h after seeding the cells were lysed and luciferase activity was measured with Dual-Luciferase Reporter Assay System (Promega). For normalization the cells were cotransfected with pRL-CMV vector (Promega) and the values of firefly luciferase activity were divided by the values of Renilla luciferase.

Statistics and Reproducibility

Sample sizes were not predetermined, the experiments were not randomized and investigators were not blinded to allocation during experiments and outcome assessment. Column statistics were performed on data sets to check for normal distribution and appropriate tests were performed. Each experiment was performed at least three times with the exception of RNA in situ hybridization for *dll4* Tg line validation (Fig. S1a,b), VEGF inhibitor treatment (Fig. S2e,f), movies of ISV sprouting (Fig. S6h,i) and blood flow analysis in ISVs of *dll4* morpholino injected embryos (Fig. S7g), which were performed two times.

Supplementary Material

Refer to Web version on PubMed Central for supplementary material.

Acknowledgements

This work was funded by the Max Planck Society (A.F.S.), the Deutsche Forschungsgemeinschaft (DFG SI-1374/3-1; DFG SI-1374/3-2; DFG SI-1374/4-1; DFG SI-1374/5-1; A.F.S.; DFG SCHN 43076-2/663; H.S.) and an ERC starting grant (260794-ZebrafishAngio; A.F.S.). This work was supported by the Deutsche Forschungsgemeinschaft (DFG) Cells-in-Motion Cluster of Excellence (EXC 1003-CIM), University of Münster, Germany (Flexible funds FF-2014-15 to A.F.S. and H.S.) and the National Institutes of Health (R01 HL093467, N.D.L.). We would like to thank Wade Sugden for critical reading of the manuscript and Jeroen Bussmann for generating the *Tg(dll4:gal4)*^{mu106} zebrafish line.

References

1. Benedito R, Hellstrom M. Notch as a hub for signaling in angiogenesis. Exp Cell Res. 2013; 319:1281–1288. [PubMed: 23328307]
2. Phng LK, Gerhardt H. Angiogenesis: a team effort coordinated by notch. Dev Cell. 2009; 16:196–208. [PubMed: 19217422]
3. Siekmann AF, Affolter M, Belting HG. The tip cell concept 10 years after: New players tune in for a common theme. Exp Cell Res. 2013
4. Jakobsson L, et al. Endothelial cells dynamically compete for the tip cell position during angiogenic sprouting. Nature cell biology. 2010; 12:943–953. [PubMed: 20871601]
5. Lobov IB, et al. Delta-like ligand 4 (Dll4) is induced by VEGF as a negative regulator of angiogenic sprouting. Proc Natl Acad Sci U S A. 2007; 104:3219–3224. [PubMed: 17296940]
6. Ubezio B, et al. Synchronization of endothelial Dll4-Notch dynamics switch blood vessels from branching to expansion. eLife. 2016; 5
7. Hellstrom M, et al. Dll4 signalling through Notch1 regulates formation of tip cells during angiogenesis. Nature. 2007; 445:776–780. [PubMed: 17259973]
8. Leslie JD, et al. Endothelial signalling by the Notch ligand Delta-like 4 restricts angiogenesis. Development. 2007; 134:839–844. [PubMed: 17251261]

9. Siekmann AF, Lawson ND. Notch signalling limits angiogenic cell behaviour in developing zebrafish arteries. Nature. 2007; 445:781–784. [PubMed: 17259972]
10. Suchting S, et al. The Notch ligand Delta-like 4 negatively regulates endothelial tip cell formation and vessel branching. Proc Natl Acad Sci U S A. 2007; 104:3225–3230. [PubMed: 17296941]
11. Lawson ND, et al. Notch signaling is required for arterial-venous differentiation during embryonic vascular development. Development. 2001; 128:3675–3683. [PubMed: 11585794]
12. Lawson ND, Vogel AM, Weinstein BM. sonic hedgehog and vascular endothelial growth factor act upstream of the Notch pathway during arterial endothelial differentiation. Dev Cell. 2002; 3:127–136. [PubMed: 12110173]
13. Duarte A, et al. Dosage-sensitive requirement for mouse Dll4 in artery development. Genes Dev. 2004; 18:2474–2478. [PubMed: 15466159]
14. Gale NW, et al. Haploinsufficiency of delta-like 4 ligand results in embryonic lethality due to major defects in arterial and vascular development. Proc Natl Acad Sci U S A. 2004; 101:15949–15954. [PubMed: 15520367]
15. Krebs LT, et al. Haploinsufficient lethality and formation of arteriovenous malformations in Notch pathway mutants. Genes Dev. 2004; 18:2469–2473. [PubMed: 15466160]
16. Bussmann J, Wolfe SA, Siekmann AF. Arterial-venous network formation during brain vascularization involves hemodynamic regulation of chemokine signaling. Development. 2011; 138:1717–1726. [PubMed: 21429983]
17. Strasser GA, Kaminker JS, Tessier-Lavigne M. Microarray analysis of retinal endothelial tip cells identifies CXCR4 as a mediator of tip cell morphology and branching. Blood. 2010; 115:5102–5110. [PubMed: 20154215]
18. del Toro R, et al. Identification and functional analysis of endothelial tip cell-enriched genes. Blood. 2010; 116:4025–4033. [PubMed: 20705756]
19. Kidoya H, et al. APJ Regulates Parallel Alignment of Arteries and Veins in the Skin. Dev Cell. 2015; 33:247–259. [PubMed: 25920569]
20. Xu C, et al. Arteries are formed by vein-derived endothelial tip cells. Nature communications. 2014; 5:5758.
21. Kiefer F, Siekmann AF. The role of chemokines and their receptors in angiogenesis. Cellular and Molecular Life Sciences. 2011; 68:2811–2830. [PubMed: 21479594]
22. Nagasawa T. CXC chemokine ligand 12 (CXCL12) and its receptor CXCR4. J Mol Med (Berl). 2014; 92:433–439. [PubMed: 24722947]
23. Ara T, Tokoyoda K, Okamoto R, Koni PA, Nagasawa T. The role of CXCL12 in the organ-specific process of artery formation. Blood. 2005; 105:3155–3161. [PubMed: 15626744]
24. Tachibana K, et al. The chemokine receptor CXCR4 is essential for vascularization of the gastrointestinal tract. Nature. 1998; 393:591–594. [PubMed: 9634237]
25. Fujita M, et al. Assembly and patterning of the vascular network of the vertebrate hindbrain. Development. 2011; 138:1705–1715. [PubMed: 21429985]
26. Siekmann AF, Standley C, Fogarty KE, Wolfe SA, Lawson ND. Chemokine signaling guides regional patterning of the first embryonic artery. Gene Dev. 2009; 23:2272–2277. [PubMed: 19797767]
27. Harrison MR, et al. Chemokine-guided angiogenesis directs coronary vasculature formation in zebrafish. Dev Cell. 2015; 33:442–454. [PubMed: 26017769]
28. Ivins S, et al. The CXCL12/CXCR4 Axis Plays a Critical Role in Coronary Artery Development. Dev Cell. 2015; 33:455–468. [PubMed: 26017770]
29. Li W, et al. Peripheral nerve-derived CXCL12 and VEGF-A regulate the patterning of arterial vessel branching in developing limb skin. Dev Cell. 2013; 24:359–371. [PubMed: 23395391]
30. Isogai S, Horiguchi M, Weinstein BM. The vascular anatomy of the developing zebrafish: an atlas of embryonic and early larval development. Dev Biol. 2001; 230:278–301. [PubMed: 11161578]
31. Kaufman R, et al. Development and origins of zebrafish ocular vasculature. BMC Dev Biol. 2015; 15:18. [PubMed: 25888280]
32. Kochhan E, et al. Blood Flow Changes Coincide with Cellular Rearrangements during Blood Vessel Pruning in Zebrafish Embryos. PLoS One. 2013; 8:e75060. [PubMed: 24146748]

33. Claxton S, Fruttiger M. Periodic Delta-like 4 expression in developing retinal arteries. Gene Expr Patterns. 2004; 5:123–127. [PubMed: 15533827]
34. Hofmann JJ, Luisa Iruela-Arispe M. Notch expression patterns in the retina: An eye on receptor-ligand distribution during angiogenesis. Gene Expr Patterns. 2007; 7:461–470. [PubMed: 17161657]
35. Quillien A, et al. Distinct Notch signaling outputs pattern the developing arterial system. Development. 2014; 141:1544–1552. [PubMed: 24598161]
36. Ninov N, Borius M, Stainier DY. Different levels of Notch signaling regulate quiescence, renewal and differentiation in pancreatic endocrine progenitors. Development. 2012; 139:1557–1567. [PubMed: 22492351]
37. Li X, et al. Generation of destabilized green fluorescent protein as a transcription reporter. J Biol Chem. 1998; 273:34970–34975. [PubMed: 9857028]
38. Bray SJ. Notch signalling in context. Nat Rev Mol Cell Biol. 2016; 17:722–735. [PubMed: 27507209]
39. Coumailleau F, Furthauer M, Knoblich JA, Gonzalez-Gaitan M. Directional Delta and Notch trafficking in Sara endosomes during asymmetric cell division. Nature. 2009; 458:1051–1055. [PubMed: 19295516]
40. Costa G, et al. Asymmetric division coordinates collective cell migration in angiogenesis. Nature cell biology. 2016; 18:1292–1301. [PubMed: 27870831]
41. Itoh M, et al. Mind bomb is a ubiquitin ligase that is essential for efficient activation of Notch signaling by Delta. Dev Cell. 2003; 4:67–82. [PubMed: 12530964]
42. Sainson RC, et al. Cell-autonomous notch signaling regulates endothelial cell branching and proliferation during vascular tubulogenesis. Faseb J. 2005; 19:1027–1029. [PubMed: 15774577]
43. Packham IM, et al. Microarray profiling reveals CXCR4a is downregulated by blood flow in vivo and mediates collateral formation in zebrafish embryos. Physiol Genomics. 2009; 38:319–327. [PubMed: 19509081]
44. Isogai S, Lawson ND, Torrealday S, Horiguchi M, Weinstein BM. Angiogenic network formation in the developing vertebrate trunk. Development. 2003; 130:5281–5290. [PubMed: 12954720]
45. De Bock K, et al. Role of PFKFB3-driven glycolysis in vessel sprouting. Cell. 2013; 154:651–663. [PubMed: 23911327]
46. Williams CK, et al. Regulation of CXCR4 by the Notch ligand delta-like 4 in endothelial cells. Cancer Res. 2008; 68:1889–1895. [PubMed: 18339870]
47. le Noble F, et al. Flow regulates arterial-venous differentiation in the chick embryo yolk sac. Development. 2004; 131:361–375. [PubMed: 14681188]
48. Serra H, et al. PTEN mediates Notch-dependent stalk cell arrest in angiogenesis. Nature communications. 2015; 6:7935.
49. Pitulescu ME. Dll4 and Notch signalllig couples sprouting angiogenesis and artery formation. Nature cell biology. 2017; XXX:XXX.
50. Noguera-Troise I, et al. Blockade of Dll4 inhibits tumour growth by promoting non-productive angiogenesis. Nature. 2006; 444:1032–1037. [PubMed: 17183313]
51. Westerfield, M. The zebrafish book : a guide for the laboratory use of zebrafish (Brachydanio rerio). M. Westerfield; Eugene, OR: 1993.
52. Kimmel CB, Ballard WW, Kimmel SR, Ullmann B, Schilling TF. Stages of embryonic development of the zebrafish. Dev Dyn. 1995; 203:253–310. [PubMed: 8589427]
53. Wang Y, et al. Moesin1 and Ve-cadherin are required in endothelial cells during in vivo tubulogenesis. Development. 2010; 137:3119–3128. [PubMed: 20736288]
54. Asakawa K, et al. Genetic dissection of neural circuits by Tol2 transposon-mediated Gal4 gene and enhancer trapping in zebrafish. Proc Natl Acad Sci U S A. 2008; 105:1255–1260. [PubMed: 18202183]
55. Parsons MJ, et al. Notch-responsive cells initiate the secondary transition in larval zebrafish pancreas. Mech Dev. 2009; 126:898–912. [PubMed: 19595765]

56. Qian F, et al. Microarray analysis of zebrafish cloche mutant using amplified cDNA and identification of potential downstream target genes. Dev Dyn. 2005; 233:1163–1172. [PubMed: 15937927]
57. Roman BL, et al. Disruption of acvrl1 increases endothelial cell number in zebrafish cranial vessels. Development. 2002; 129:3009–3019. [PubMed: 12050147]
58. Hogan BM, et al. ccbe1 is required for embryonic lymphangiogenesis and venous sprouting. Nature Genetics. 2009; 41:396–398. [PubMed: 19287381]
59. Lawson ND, Weinstein BM. In vivo imaging of embryonic vascular development using transgenic zebrafish. Dev Biol. 2002; 248:307–318. [PubMed: 12167406]
60. Bussmann J, et al. Arteries provide essential guidance cues for lymphatic endothelial cells in the zebrafish trunk. Development. 2010; 137:2653–2657. [PubMed: 20610484]
61. Traver D, et al. Transplantation and in vivo imaging of multilineage engraftment in zebrafish bloodless mutants. Nature Immunology. 2003; 4:1238–1246. [PubMed: 14608381]
62. Jiang YJ, et al. Mutations affecting neurogenesis and brain morphology in the zebrafish, Danio rerio. Development. 1996; 123:205–216. [PubMed: 9007241]
63. Scheer N, Campos-Ortega JA. Use of the Gal4-UAS technique for targeted gene expression in the zebrafish. Mech Dev. 1999; 80:153–158. [PubMed: 10072782]
64. Bussmann J, Schulte-Merker S. Rapid BAC selection for tol2-mediated transgenesis in zebrafish. Development. 2011; 138:4327–4332. [PubMed: 21865323]
65. Hermkens DM, et al. Sox7 controls arterial specification in conjunction with hey2 and efnb2 function. Development. 2015; 142:1695–1704. [PubMed: 25834021]
66. Bahary N, et al. Duplicate VegfA genes and orthologues of the KDR receptor tyrosine kinase family mediate vascular development in the zebrafish. Blood. 2007; 110:3627–3636. [PubMed: 17698971]
67. Kochhan, E., Siekmann, AF. Zebrafish as a Model to Study Chemokine Function. Chemokines: Methods and Protocols. Cardona, EA., Ubogu, EE., editors. Humana Press; Totowa, NJ: 2013. p. 145-159.
68. Brend T, Holley SA. Zebrafish whole mount high-resolution double fluorescent in situ hybridization. J Vis Exp. 2009
69. Moore JC, et al. Post-transcriptional mechanisms contribute to Etv2 repression during vascular development. Dev Biol. 2013; 384:128–140. [PubMed: 24036310]
70. Ulrich F, Ma LH, Baker RG, Torres-Vazquez J. Neurovascular development in the embryonic zebrafish hindbrain. Dev Biol. 2011; 357:134–151. [PubMed: 21745463]
71. Kronstein R, et al. Caveolin-1 opens endothelial cell junctions by targeting catenins. Cardiovasc Res. 2012; 93:130–140. [PubMed: 21960684]

Europe PMC Funders Author Manuscripts

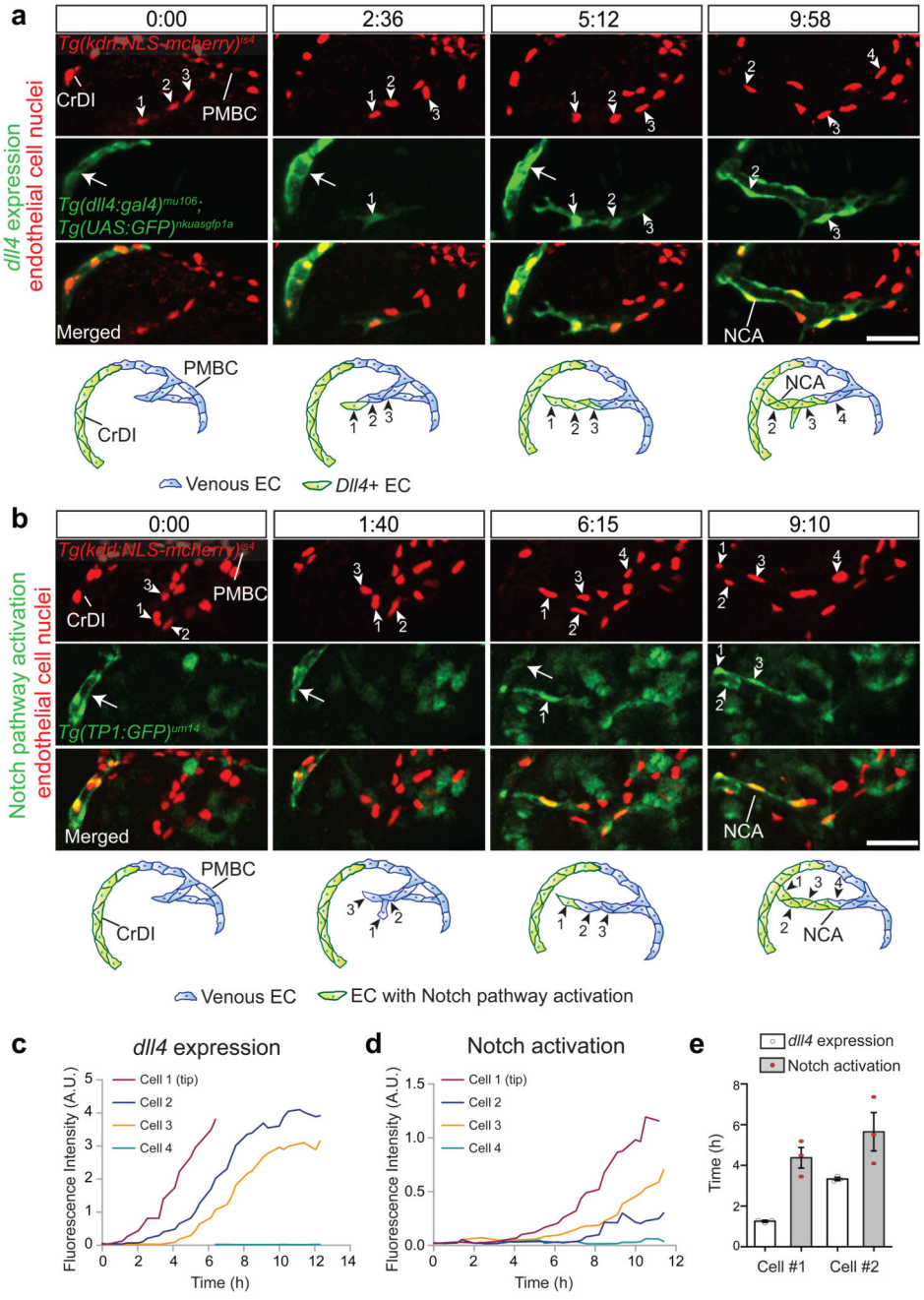

Figure 1. Time-lapse imaging of *dll4* and Notch reporter lines during blood vessel development.

(a) Still images at indicated time points of NCA sprouting from the venous PMBC and connecting to the arterial CrDI in *Tg(dll4:gal4)*^{mu106}; *Tg(UAS:GFP)*^{nkuasgfp1a}, a *dll4* expression reporter (green), and *Tg(kdrl:NLS-mcherry)*^{is4}, which marks all EC nuclei in red, triple transgenic embryos (n=3 embryos). White arrowheads with numbers mark individual ECs. Note onset of GFP expression in cell number 1 at the 2:36 h time point, followed by GFP expression in cells 2 and 3. Arrows point to CrDI. **(b)** Still images at indicated time points of NCA sprouting in *Tg(TP1:GFP)*^{um14}, a reporter for Notch signalling pathway

activation, and *Tg(kdrl:NLS-mcherry)*^{is4} double transgenic embryos (n=3 embryos).White arrowheads with numbers mark individual ECs. Note onset of GFP expression in cell number 1 at the 6:15 h time point, followed by GFP expression in cells 2 and 3. Arrows point to CrDI. **(c)** Quantification of fluorescence intensity of the green *Tg(dll4:gal4)*^{mu106}; *Tg(UAS:GFP)*^{nkuasgfp1a} signal normalized to red *Tg(kdrl:NLS-mcherry)*^{is4} signal over time. **(d)** Quantification of fluorescence intensity of the green *Tg(TP1:GFP)*^{um14} signal normalized to red *Tg(kdrl:NLS-mcherry)*^{is4} signal over time. **(e)** Comparison of onset of *dll4* expression and Notch pathway activation in tip and stalk cells in *Tg(dll4:gal4)*^{mu106}; *Tg(UAS:GFP)*^{nkuasgfp1a}; *Tg(TP1:H2B-mcherry)*^{s939} triple transgenic embryos (See Supplementary Fig. 4) (n=3 embryos, 3 independent experiments). Wilcoxon matched pairs-signed rank test. Error bars: Mean ± s.e.m. Videos are representative of three independent experiments. t_0 = 26 hpf. Scale bars, 50 μm. A.U.-arbitrary units; CrDI-cranial division of the internal carotid artery; EC-endothelial cell; h-hour; hpf-hours post fertilization; NCA-nasal ciliary artery; PMBC-primordial midbrain channel.

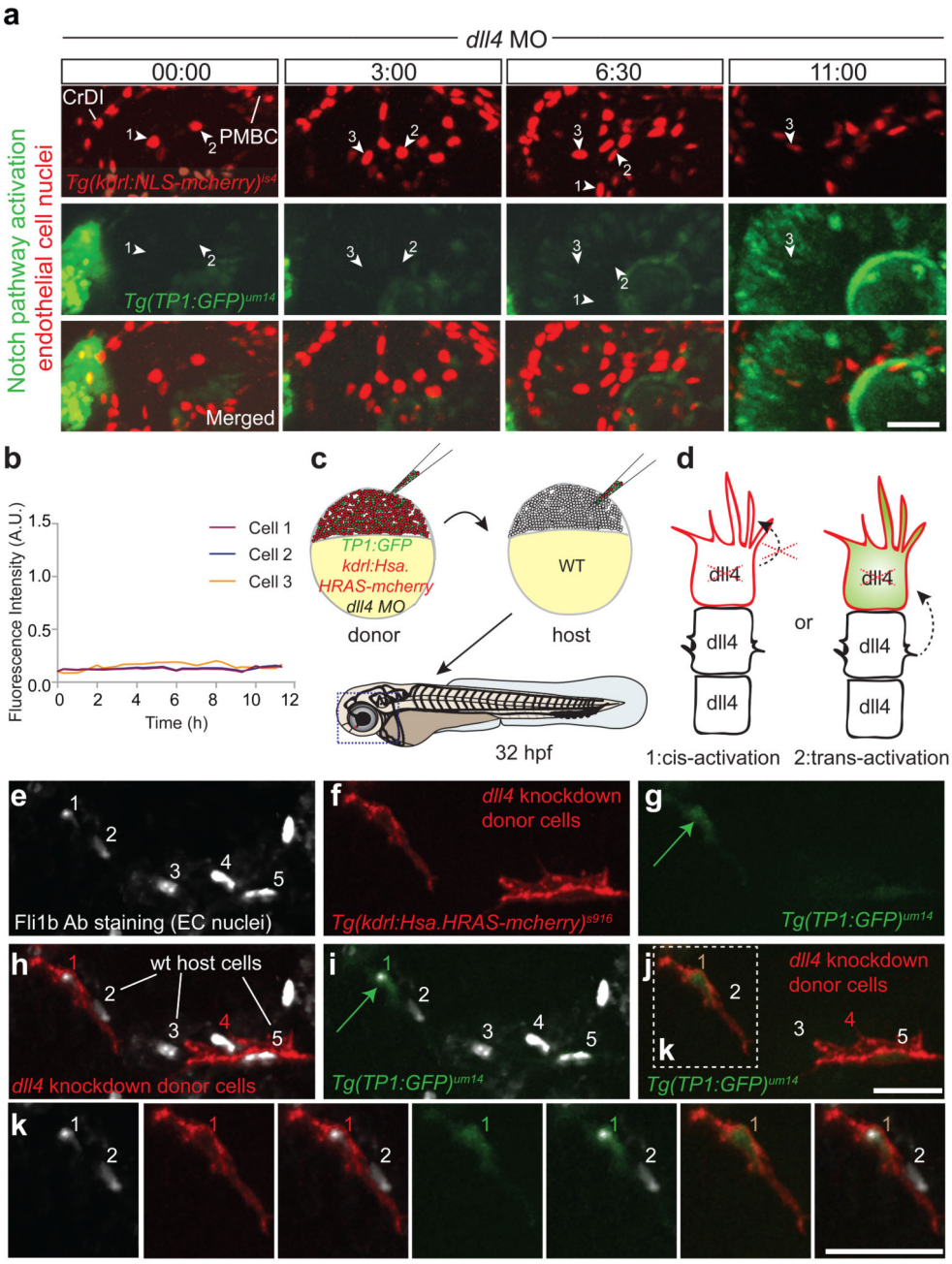

Figure 2. Dll4 trans activates Notch signalling in tip cells.

(a) Representative images from time-lapse analysis of Notch reporter *Tg(TP1:GFP)*^{um14}, marking cells with active Notch signalling in green and endothelial nuclear marker *Tg(kdrl:NLS-mcherry)*^{is4}, marking EC nuclei in red, double transgenic embryos injected with *dll4* MO. **(b)** Quantification of fluorescent intensity of the green *Tg(TP1:GFP)*^{um14} signal normalized to red *Tg(kdrl:NLS-mcherry)*^{is4} signal over time. t_0 = 26 hpf. (n=3 embryos, 3 independent experiments) **(c)** Transplantation scheme. *Tg(kdrl:Hsa.HRAS-mcherry)*^{s916} marks EC membranes of donor cells in red, while *Tg(TP1:GFP)*^{um14} marks

Europe PMC Funders Author Manuscripts

donor cells with Notch signalling pathway activation in green. **(d)** Schematic detailing different outcomes of cell transplantations. Transferring *dll4* knockdown cells from *Tg(kdrl:Hsa.HRAS-mcherry)*^{s916}; *Tg(TP1:GFP)*^{um14} into wt hosts allows for distinguishing trans- from cis-activation of Notch signalling in ECs. **(e)** NCA cells stained with a Fli1b antibody detecting endothelial cell nuclei (white) (n=3 mosaic embryos with single donor cell at tip position, 3 independent experiments). **(f)** Transplanted *dll4* knockdown ECs (red). **(g)** Tip cell with activated Notch signalling identified via GFP expression (green arrow). **(h)** Overlay of transplanted NCA cells with host NCA cells, showing that cells 1 and 4 are donor-derived, while cells 2, 3 and 5 are host-derived. **(i)** Overlay of transplanted cells showing Notch pathway activation (green arrow) in host cells. Only the tip cell (number 1) shows GFP expression. **(j)** Overlay image, identifying transplanted *dll4* knockdown tip cell being GFP positive. **(k)** Zoom in of boxed area in j. Note tip cell (number 1) being next to a wt host cell. Scale bars, 50 μm. A.U.-arbitrary units; CrDI-cranial division of the internal carotid artery; EC-endothelial cell; h-hour; hpf-hours post fertilization; MO-morpholino; NCA-nasal ciliary artery; PMBC-primordial midbrain channel.

Europe PMC Funders Author Manuscripts

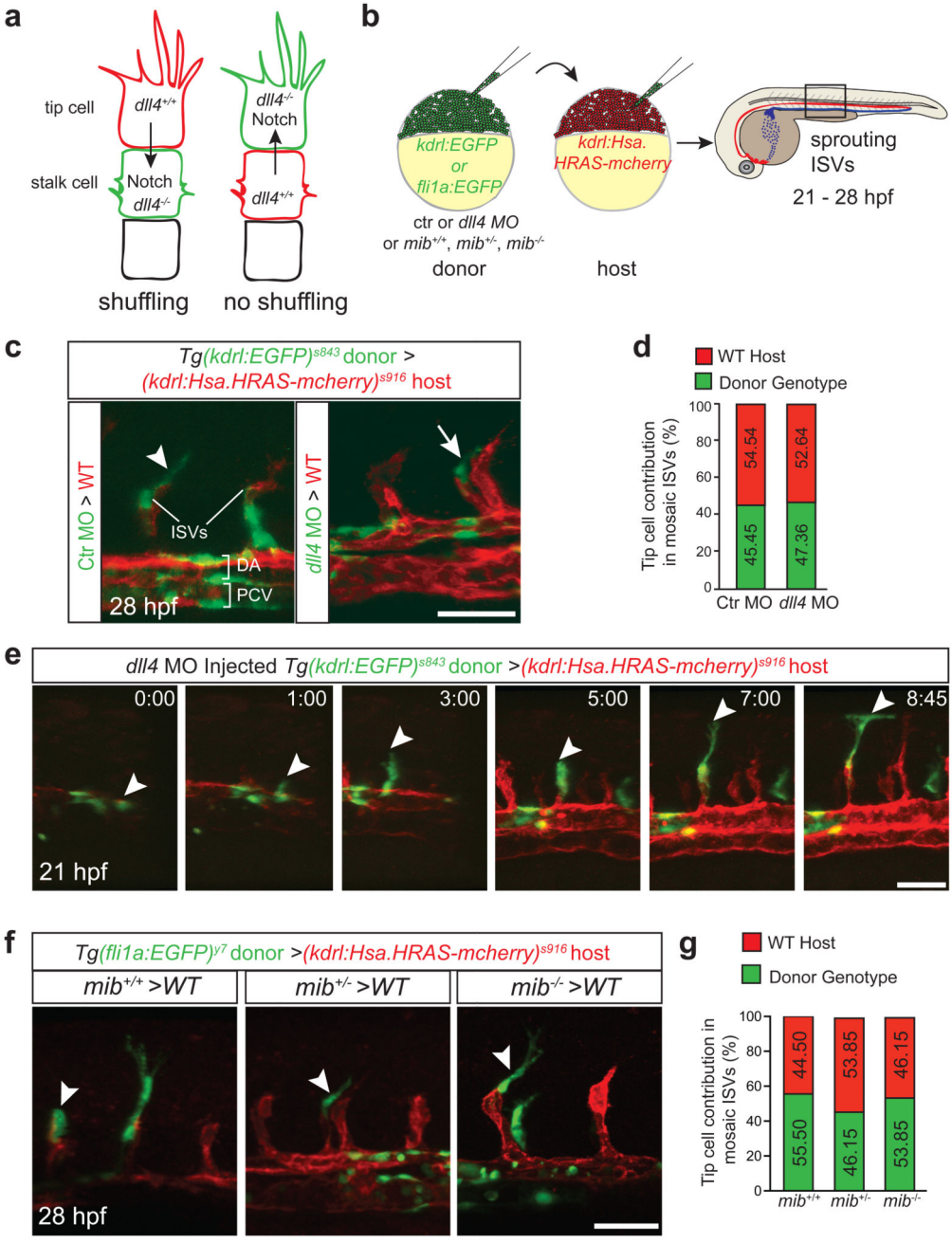

Figure 3. Notch signalling does not mediate competition between endothelial cells during intersegmental blood vessel sprouting.

(a) Schematic drawing illustrating expected positions of ECs with indicated genotypes within blood vessel sprouts if *dll4* would be required to activate Notch signalling in stalk cells (shuffling) or in tip cells (no shuffling). **(b)** Schematic drawing of transplantation procedure. **(c)** Representative image of transplanted MO injected donor EC in ISVs at 28 hpf. Arrowhead marks transplanted ctr MO injected cell, while arrow marks *dll4* MO injected cell. DA and PCV are indicated. *Tg(kdrl:EGFP)*^{s843} marks donor cells by virtue of

cytoplasmic EGFP expression in green, while *Tg(kdrl:Hsa.HRAS-mcherry)*^{s916} marks host cells by virtue of membrane mcherry expression in red. **(d)** Quantification of tip cell contribution of ctr MO (n=21 mosaic ISVs from 17 embryos) or *dll4* MO (n=19 mosaic ISVs from 15 embryos) injected donor cells (four independent experiments). **(e)** Time-lapse imaging of mosaic ISV sprouts showing *dll4* MO injected cell maintaining the tip cell position (arrowheads; n=3 embryos, 3 independent experiments). **(f)** Still images showing ECs with indicated *mib* genotype maintaining tip cell positions (arrowheads). **(g)** Quantification of tip cell contribution of wt (n=9 mosaic ISVs from 7 embryos), *mib* heterozygous (n=26 mosaic ISVs from 19 embryos) or homozygous (n=13 mosaic ISVs from 9 embryos) mutant donor cells (four independent experiments). Scale bars, 50 μm. Ctr-control; DA-dorsal aorta; EC-endothelial cell; hpf-hours post fertilization; ISV-intersegmental blood vessel; MO-morpholino; PCV-posterior cardinal vein; wt-wild type.

Europe PMC Funders Author Manuscripts

Europe PMC Funders Author Manuscripts

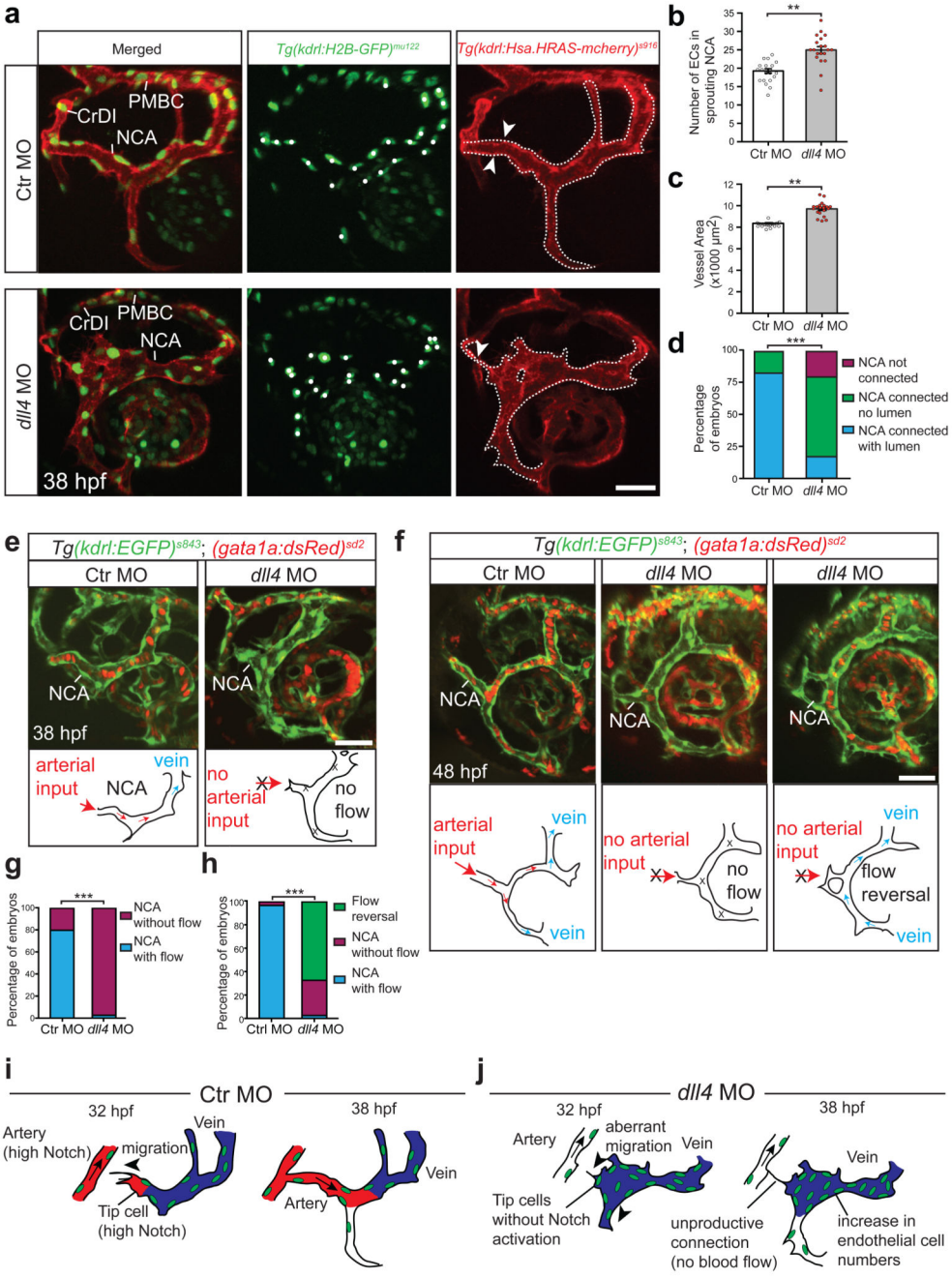

Figure 4. Loss of Notch signalling in sprouting ECs causes vascular hyperplasia and aberrant arterial-venous connections.

(a) NCA phenotypes in *dll4* MO injected *Tg(kdrl:H2B-GFP)*^{mu122}, marking all EC nuclei in green and *Tg(kdrl:Hsa.HRAS-mcherry)*^{s916}, marking EC membranes in red, double transgenic embryos. White dots indicate EC nuclei, white dotted lines outline vessel areas. Arrowheads mark connected and perfused NCA in ctr MO condition (2 arrowheads), while in *dll4* MO injected embryos, NCA connections were dysmorphic (one arrowhead). **(b, c, d)** Quantification of NCA **(b)** EC numbers, **(c)** area and **(d)** NCA-CrDI connections in ctr MO

(n=20) and *dll4* MO (n=20) injected embryos. **(e)** NCA blood flow at the 38 hpf time point in ctr and *dll4* MO injected embryos visualized using *Tg(gata1:dsRed)*^{sd2} embryos. Note blood flow from artery to vein. *Tg(kdrl:EGFP)*^{s843} marks EC in green. *Tg(gata1a:dsRed)*^{sd2} marks erythrocytes in red. Lack of NCA-CrDI connection leads to absence of blood flow in *dll4* MO injected embryos. **(f)** NCA blood flow at the 48 hpf time point in ctr and *dll4* MO injected embryos. Note blood flow from artery into two veins. Lack of NCA-CrDI connection in *dll4* MO injected embryos causes aberrant blood flow patterns, including flow reversal due to direct connection of two veins. **(g)** Quantification of NCA flow defects in ctr (n=30) and *dll4* MO (n=30) injected embryos at 38 hpf **(h)** Quantification of NCA flow defects in ctr (n=30) and *dll4* MO (n=30) injected embryos at 48 hpf. **(i)** Schematic drawing of NCA-CrDI connection in ctr MO injected embryos. Black arrows denote blood flow direction, black arrowheads indicate direction of EC migration. **(j)** Schematic drawing of NCA-CrDI connection in *dll4* MO injected embryos. Black arrows denote blood flow direction, black arrowheads indicate direction of EC migration. Images are representative of three independent experiments. Error bars: Mean ± s.e.m. For **4b, c** **p<0.001, Unpaired Student's *t*-test with Welch's correction. For **4d, g, h** ***p<0.0001, Fischer's exact test. Scale bars, 50 μm. CrDI-cranial division of the internal carotid artery; Ctr-control; EC-endothelial cell; hpf-hours post fertilization; MO-morpholino; NCA-nasal ciliary artery; PMBC-primordial midbrain channel.

Europe PMC Funders Author Manuscripts

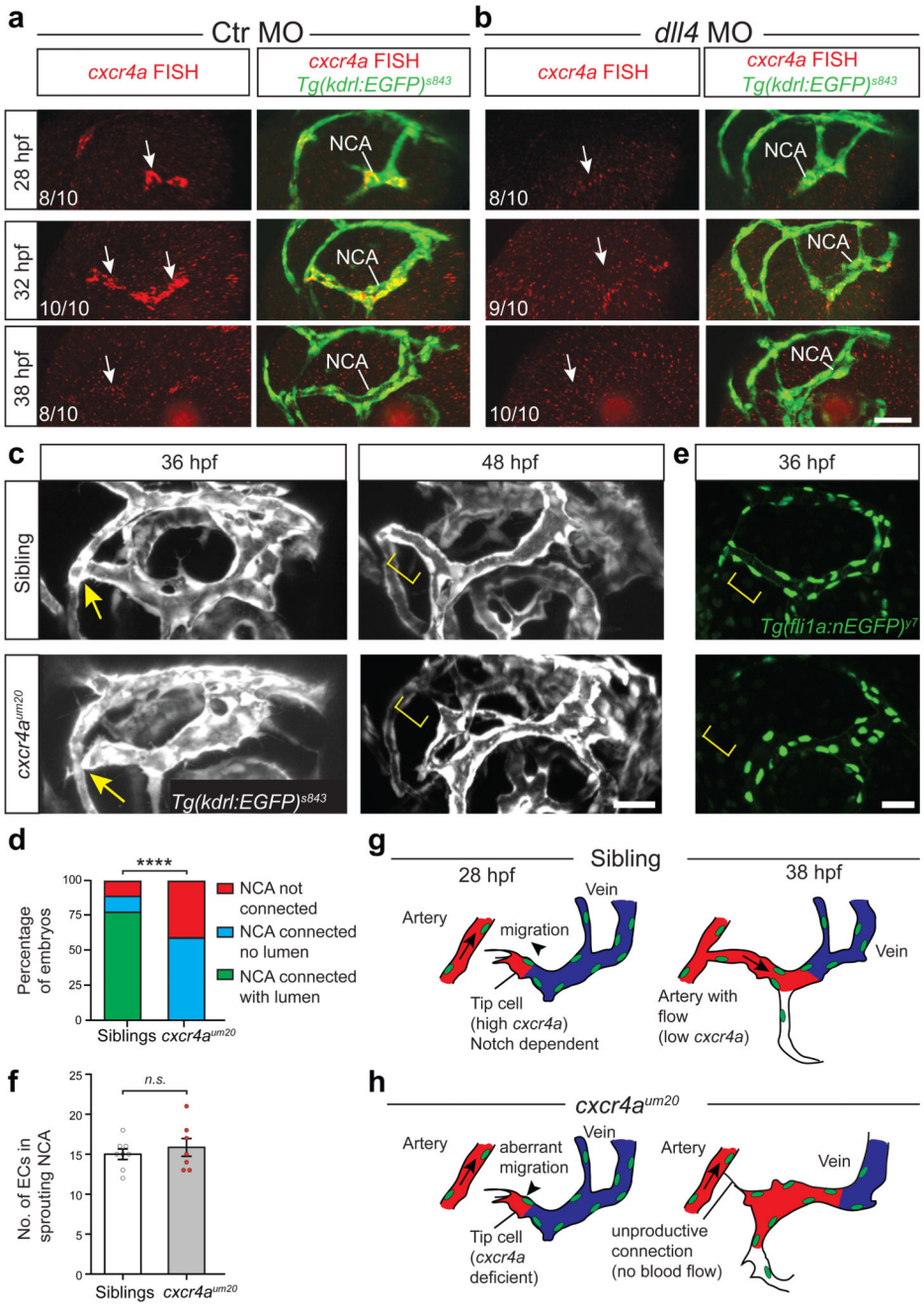

Figure 5. Notch induction of *cxcr4a* expression mediates arterial-venous connections.

(a) FISH to reveal expression of *cxcr4a* in NCA ECs in ctr MO injected embryos between 28 and 38 hpf (arrows). *Tg(kdrl:EGFP)*^{s843} marks all ECs in green. Expression of *cxcr4a* becomes downregulated in NCA cells at 38 hpf. **(b)** Expression of *cxcr4a* in *dll4* MO injected embryos is largely absent (arrows). ('*n*/*N*' reports the 'number of embryos with staining pattern in image'/'total embryos from three independent experiments', N=10 embryos for each time point.) **(c)** Loss of *cxcr4a* function causes NCA-CrDI connection defects starting at the 36 hpf time point (arrows). At 48 hpf time point NCA formation is still

impaired in *cxcr4a* mutant embryos (brackets). **(d)** Quantification of NCA-CrDI connections in sibling (n=9) and *cxcr4a* mutant (n=7) embryos at 36 hpf. **(e)** Loss of *cxcr4a* function does not lead to changes in NCA EC cell numbers, as analysed in *Tg(fli1a:nEGFP)*^{y7} fish, marking EC nuclei in green. Brackets indicate location of NCA. **(f)** Quantification of EC numbers in sibling (n=9) and *cxcr4a* mutant (n=7) embryos at 36 hpf. **(g)** Schematic drawing of *cxcr4a* expression during NCA-CrDI connection. Black arrows denote blood flow direction; black arrowheads indicate direction of EC migration. **(h)** Schematic drawing of NCA-CrDI connection defects in *cxcr4a* mutant embryos. Black arrows denote blood flow direction, black arrowheads indicate direction of EC migration. Images are representative of three independent experiments. Error bars: Mean ± s.e.m. ***p<0.0001, For **5d**, Fischer's exact test. For **5f**, Unpaired Student's *t*-test with Welch's correction. Scale bars, 50 μm in **b** and 30 μm in **c, e**. n.s.- not significant; Ctr-control; EC-endothelial cell; hpf-hours post fertilization; MO-morpholino; NCA-nasal ciliary artery.

Europe PMC Funders Author Manuscripts

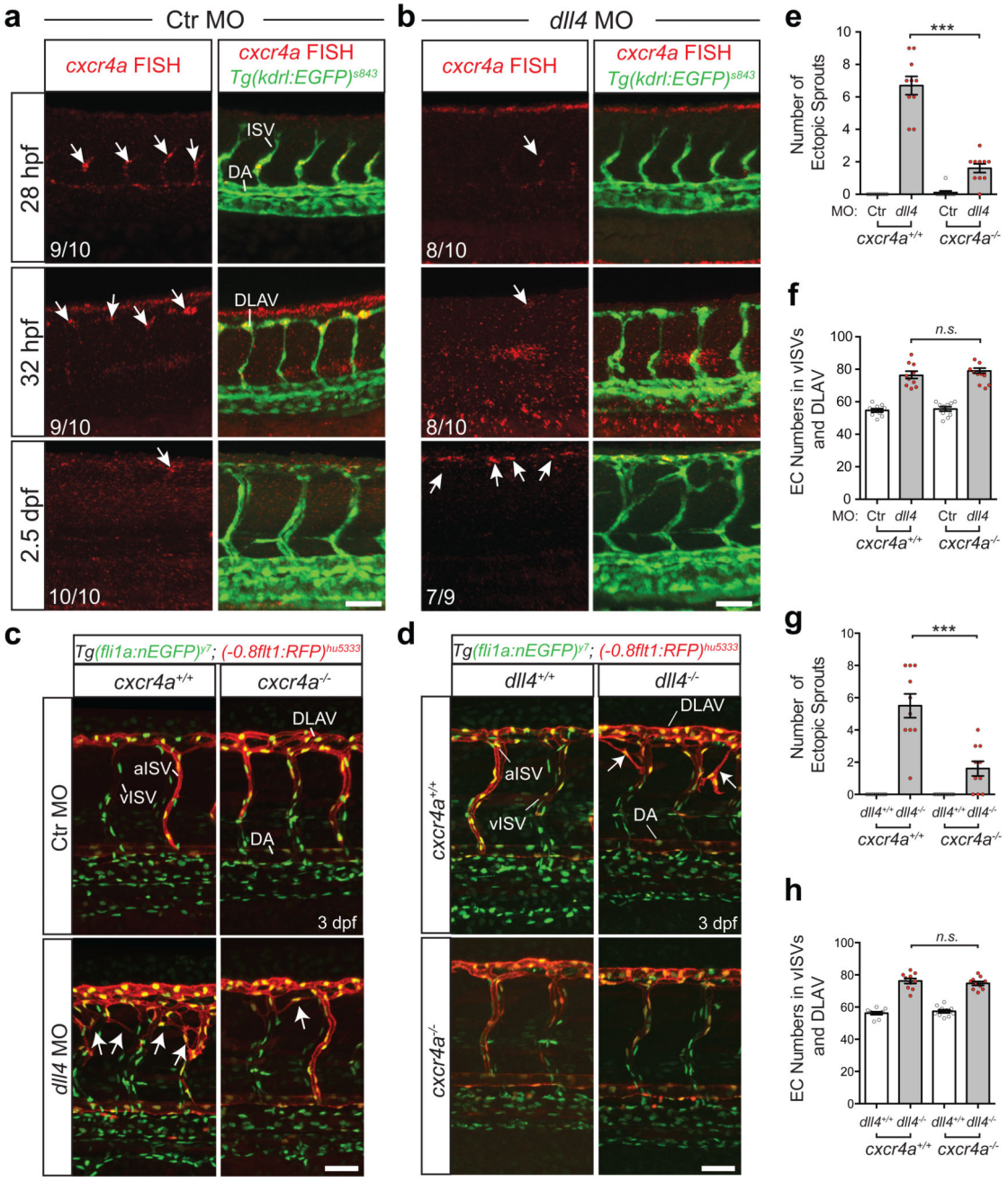

Figure 6. Aberrant *cxcr4a* expression contributes to excessive blood vessel sprouting in embryos lacking *dll4*-Notch signalling.

(a) FISH to detect *cxcr4a* expression in sprouting ISVs. Expression starts in newly forming sprouts (arrows, 28 hpf). Expression of *cxcr4a* is visible in the newly forming DLAV (arrows, 32 hpf). Subsequently, *cxcr4a* expression is being downregulated (arrow, 2.5 dpf). *Tg(kdrl:EGFP)*^{s843} marks all ECs in green. **(b)** FISH to detect *cxcr4a* expression in sprouting ISVs in *dll4* MO injected embryos. Expression is reduced in ISVs (arrow, 28 hpf) and in the newly forming DLAV (arrow, 32 hpf). Subsequently, *cxcr4a* expression is

upregulated in DLAV cells (arrows, 2.5 dpf). ('*n*/*N*' reports the 'number of embryos with staining pattern in image'/'total embryos from three independent experiments', N=10 embryos for each time point, except for **b**, where N=9 embryos.) **(c)** Loss of *cxcr4a* function can rescue excessive blood vessel sprouting in *dll4* MO injected embryos and **(d)** *dll4*^{i16e1} mutants. Representative pictures of endothelial hypersprouting (arrows) in embryos with indicated genotypes at 3 dpf. *Tg(fli:nEGFP)*^{y7} marks EC nuclei in green, while *Tg(-0.8 flt1:RFP)*^{hu5333} marks arterial ECs in red. **(e)** Quantification of ectopic sprouts in embryos (n=10) with the indicated genotypes. **(f)** Quantification of EC numbers in embryos (n=10) with the indicated genotypes. **(g)** Quantification of ectopic sprouts in embryos (n=10) with the indicated genotypes. **(h)** Quantification of EC numbers in embryos (n=10) with the indicated genotypes. Images are representative of three independent experiments. Error bars: Mean ± s.e.m. ***p<0.0001, Mann Whitney U test. Scale bars, 50 μm. n.s.- not significant; Ctr-control; DA-dorsal aorta; DLAV-dorsal longitudinal anastomotic vessel; EC-endothelial cell; FISH-fluorescent in situ hybridization; hpf-hours post fertilization; ISV-intersegmental blood vessel; MO-morpholino; vISV-venous intersegmental blood vessel.

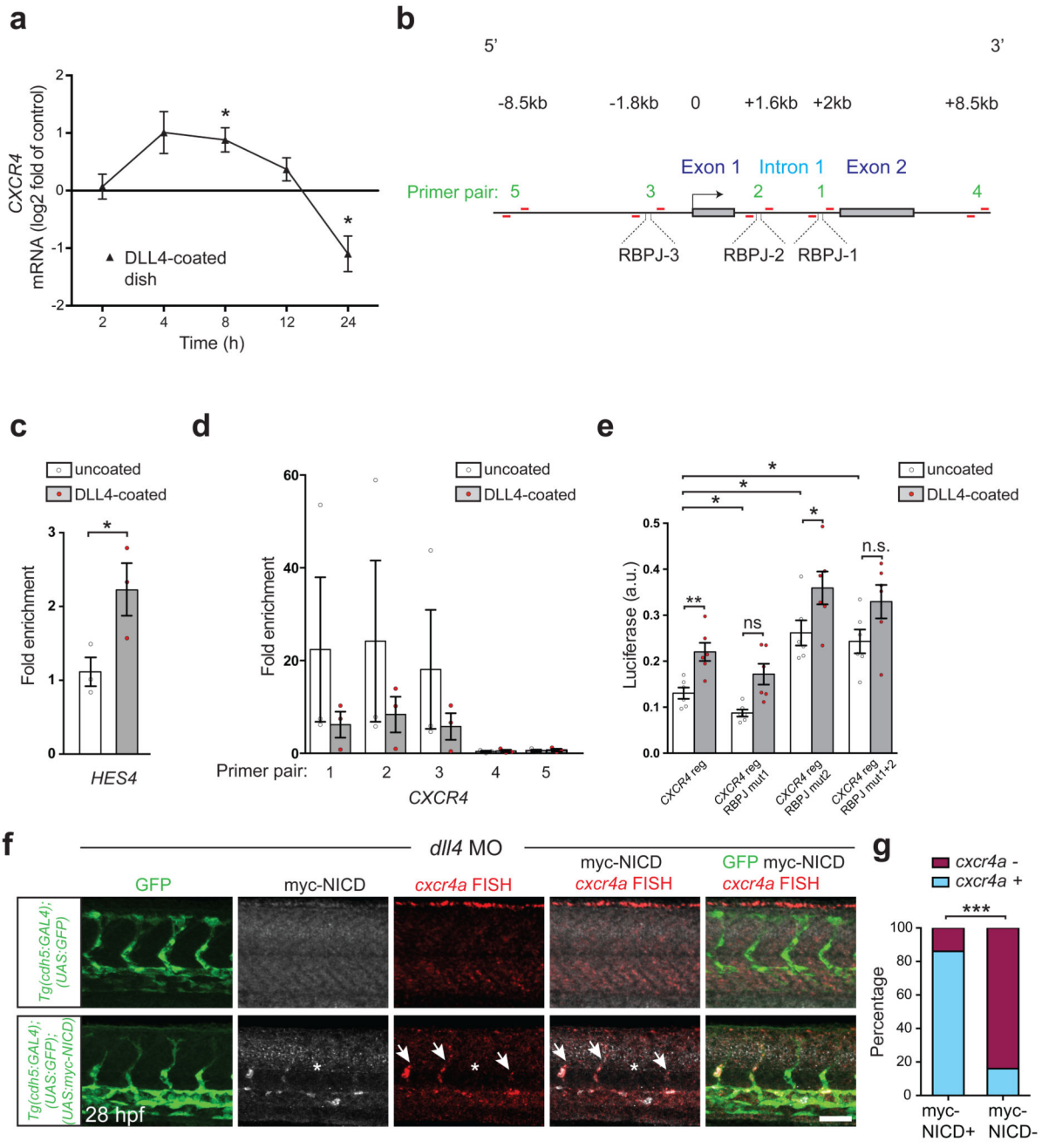

Figure 7. Regulation of *CXCR4* expression by Notch.

(a) Time course of *CXCR4* expression in HUAEC grown on DLL4-coated dishes to activate Notch signalling (n=4 independent experiments). **(b)** Schematic representation of *CXCR4* genomic locus. Rectangles represent *CXCR4* exons and the arrow represents transcription start site. The positions of identified RBPJ binding sites in *CXCR4* intron (1 and 2) and promoter (3) are shown and their positions relative to the ATG are indicated above. **(c, d)** ChIP qPCR to detect RBPJ binding in the regulatory regions of **c** *HES4* and **d** *CXCR4* (n=3 independent experiments). The cells were seeded on DLL4 for 4 h. The data are represented

as fold enrichment relative to a negative region (alpha Satellite repeat), which was set as 1. The positions of the primers amplifying RBPJ binding sites (1-3) in *CXCR4* regulatory regions, as well as the regions with no RBPJ sites (4-5) are shown in **b** as red bars. **(e)** Luciferase assay showing the response of the plasmid containing wild type *CXCR4* regulatory region (2.5 kb promoter and intron), as well as the constructs with one or two mutated RBPJ binding sites (corresponding to the numbers in **b**), to Notch activation 24 h after seeding the cells on DLL4 (n=6 independent experiments). **(f)** EC specific NICD overexpression in *dll4* MO injected *Tg(cdh5:gal4ff)*^{mu101}*; (UAS:GFP)*^{nkuasgfp1a}*; (UAS:myc-NICD)*^{kca3} triple transgenic embryos (n=10), followed by FISH and myc staining to detect *cxcr4a* and NICD expression respectively. Myc-NICD positive (+) ECs express *cxcr4a* (arrows) whereas myc-NICD negative (–) ECs do not (asterisk). **(g)** Quantification of *cxcr4a* expression in myc-NICD positive (+) and myc-NICD negative (–) ECs. Images are representative of three independent experiments. Error bars: Mean ± s.e.m. * $p<0.05$, ** $p<0.001$, *** $p<0.0001$, statistical analysis in **a, c, d** was performed using a paired two-tailed Student's *t*-test and in **g** using Fisher's exact test. In **a** the Student's *t*-test was performed at each time point by comparing control and DLL4 conditions. In **e** the data were analyzed using repeated measures one–way ANOVA and Tukey's multiple comparison test. MO-morpholino; hpf-hours post fertilization; reg-regulatory region; mut-mutated; Scale bar 50μm.

Europe PMC Funders Author Manuscripts

Europe PMC Funders Author Manuscripts

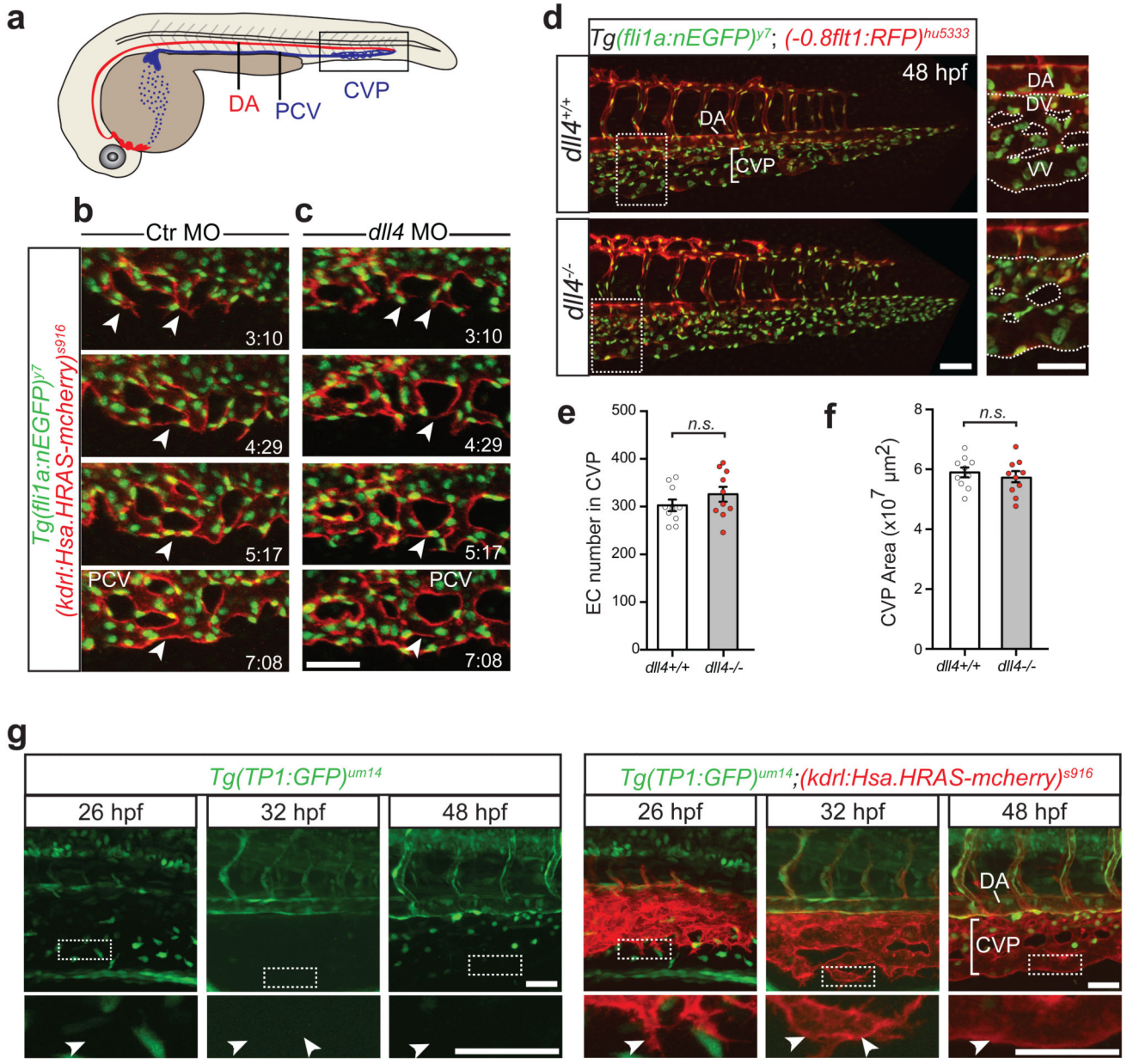

Figure 8. Venous plexus blood vessel sprouting occurs normally in the absence of Notch signalling.

(a) Schematic drawing indicating location of CVP. **(b)** Time-lapse imaging of CVP sprouting (3:10 h, arrowheads), connection between two sprouts (4:29 h, arrowhead) and lumen formation (7:08 h, arrowhead) in ctr MO injected embryo (n=3 embryos). *Tg(fli1a:nEGFP)*^{y7} marks EC nuclei in green, while *Tg(kdrl:Hsa.HRAS-mcherry)*^{s916} marks EC membranes in red. **(c)** Time-lapse imaging of CVP sprouting (3:10 h, arrowheads), connection between two sprouts (4:29 h, arrowhead) and lumen formation (7:08 h, arrowhead) in *dll4* MO injected embryo (n=3 embryos). **(d)** Comparison of CVP in wt and *dll4* mutant embryos. *Tg(fli1a:nEGFP)*^{y7} marks EC nuclei in green, while

Tg(-08.flt1:RFP)^{hu5333} marks arterial blood vessels in red. **(e)** Quantification of EC numbers in wt (n=10) and *dll4* mutant (n=10) embryos. **(f)** Quantification of CVP area in wt (n=10) and *dll4* mutant (n=10) embryos. **(g)** Analysis of Notch activation in ECs of the CVP in *Tg(TP1:GFP)*^{um14}; *Tg(kdrl:Hsa.HRAS-mcherry)*^{s916} double transgenic zebrafish (n=10 embryos). No GFP expression can be detected in ECs at any given time point (arrowheads). Videos and images are representative of three independent experiments. Error bars: Mean ± s.e.m. Unpaired *t*-test with Welch's correction. Scale bars, 50 μm. Ctr-control; CVP-caudal vein plexus; DA-dorsal aorta; DV-dorsal vein; EC-endothelial cell; hpf-hours post fertilization; MO-morpholino; PCV; posterior cardinal vein; VV-ventral vein; n.s.-not significant.

Europe PMC Funders Author Manuscripts